Image Parameter Design of Noncommensurate Distributed Structures: An Application to Microstrip Low-Pass Filters

MARIO SALERNO, MEMBER, IEEE, ROBERTO SORRENTINO, SENIOR MEMBER, IEEE, AND FRANCO GIANNINI, SENIOR MEMBER, IEEE

Abstract —**The direct application of the image parameter method (IPM) to distributed structures is suggested in order to overcome some limitations of classical design methods for microwave filters. Several advantages are pointed out: 1) Wider degrees of freedom are obtained using noncommensurate structures. 2) The IPM can be applied directly to a microwave structure without any use of lumped prototypes. 3) Possible technological constraints can be easily incorporated in the design procedure. 4) Filters designed according to the IPM can be cascaded together in order to improve their characteristics. An application to the design of a class of microstrip low-pass filters, which have been previously designed on a low-frequency approximation basis, is illustrated in detail. The IPM is shown to provide an effective control of both the passband and stopband, leading to filters with improved characteristics, as demonstrated by the experimental results.**

I. Introduction

THE BASIC PHILOSOPHY in the design of microwave filters may be regarded as consisting schematically of the following steps: 1) synthesis of a suitable lumped prototype; 2) transformation of the lumped prototype into a distributed (transmission-line) prototype; and 3) transformation of the distributed prototype into a microwave structure.

The actual design procedure may not go explicitly through each of the above steps, some of them, specifically 2) and 3), being possibly grouped together. In any case, the microwave filter design ultimately resides on a lumped filter synthesis because of the lack of approximation methods for general distributed networks; in fact, some transformation procedure (step 2)) is needed in order to establish a mathematical link between the distributed structure and the lumped network, for which well-established approximation theories are available. This transformation can be either exact, as Richard's transformation, or approximate. Both cases have some disadvantages.

In the first case, all the degrees of freedom of the distributed structure are not fully exploited since such a procedure results in some constraints on the microwave filter structure. The application of Richard's transformation, for instance, gives rise to distributed filters consisting of line sections of the same length. These constraints not only limit the degrees of freedom of the microwave structure, but may also be incompatible with some technological limitations. The synthesis procedure may end up with some characteristic impedances which are unrealizable with a given technology, e.g., the microstrip technology.

If an approximate transformation is used in step 2), this will affect the actual behavior of the microwave filter. An additional source of approximation is involved in the transformation from distributed to microwave structures (step 3)). These approximations may limit the bandwidth of the filter and/or, in general, its electrical performance.

The above disadvantages can be removed by adopting a design procedure operating directly on the microwave structure. Lacking a general approximation theory for distributed noncommensurate structures, it is very advantageous to adopt the image parameter method (IPM).

The IPM, as is known, is not an exact procedure and does not provide an *a priori* knowledge of the performance of the filter when it is terminated by resistances. Moreover, its application requires a good deal of cut and try. In the design of lumped filters, the insertion-loss method is therefore certainly preferable.

Contrary to the insertion-loss method, however, the IPM can be applied directly to a distributed or microwave structure without any considerations of lumped prototypes, so that the above-mentioned limitations can be, in principle, eliminated. Strangely enough, in spite of the fact that the image viewpoint is a wave viewpoint, this method has been generally applied only to the design of lumped-element filters [1]. On the contrary, this method is, in our opinion, very attractive for the design of microwave filters. By this technique, the reliability of the design resides only on the accuracy of the modeling of the microwave structure, not on the transformation from a lumped to a distributed prototype. In addition, because of the greater flexibility, the technological constraints can be easily incorporated in the design procedure. Finally, cut and dry problems, which could have discouraged the use of the IPM in the past, can now be easily managed thanks to modern computing facilities. In most cases, the design procedure can be implemented on a desk-top computer.

Manuscript received November 14, 1984; revised August 8, 1985.

M. Salerno and R. Sorrentino are with the University of Rome La Sapienza, Via Eudossiana no. 18, 00184 Rome, Italy.

F. Giannini is with the University of Rome Tor Vergata, Via O. Raimondo, 00173 Rome, Italy.

IEEE Log Number 8405927.

0018-9480/86/0100-0058$01.00 ©1986 IEEE

ances and image propagation constants are given by

$$Z_{II} = r_l\sqrt{B/A}$$
$$Z_{Is} = r_l/\sqrt{A\cdot B}$$
$$\cosh\gamma = c_{2l} + (r_l/r_s)s_{2l}t_s \tag{2}$$

where

$$A = 1 + r_l t_s/(r_s t_l)$$
$$B = 1 + r_l t_l t_s/r_s \tag{3}$$
$$t_l = \tanh(\tau_l s)$$
$$t_s = \tanh(\tau_s s)$$
$$c_{2l} = \cosh(2\tau_l s)$$
$$s_{2l} = \sinh(2\tau_l s) \tag{4}$$

and s is the complex radian frequency. Because of the lossless character of the cell, the frequency axis can be subdivided into passbands and stopbands, where the image impedances are purely real or imaginary, respectively. Correspondingly, the image propagation constant is imaginary in the passbands and real (apart from a constant imaginary term) in the stopbands. The cutoff frequencies are obtained from the following transcendental equations:

$$\rho\tan\left(\frac{\pi}{2}f/f_s\right)\tan\left(\frac{\pi}{2}f/f_l\right) = 1 \tag{5a}$$

$$\rho\tan\left(\frac{\pi}{2}f/f_s\right) + \tan\left(\frac{\pi}{2}f/f_l\right) = 0 \tag{5b}$$

$$\sin(\pi f/f_l) = 0 \tag{5c}$$

where

$$f_s = 1/(4\tau_s)$$
$$f_l = 1/(4\tau_l) \tag{6}$$

and

$$\rho = r_l/r_s \tag{7}$$

is the impedance ratio of the cell. The graphical solutions of (5a) and (5b) are given in Fig. 3 (a) and (b) for the two cases $f_s < f_l$ and $f_s > f_l$. The roots of (5c) are obviously $f = mf_l$ $(m = 1,2,\ldots)$.

Because of the distributed character of the cell, its frequency behavior is a complicated function of the parameters of the cell itself. In any case, the following general properties can be deduced.

1) A passband is always located next to the zero frequency and extends up to the first cutoff frequency f_{c1}, which is given by the first root of (5a).

2) For $f_s < f_l$, thus $\tau_s > \tau_l$ (Fig. 3(a)), the second cutoff frequency f_{c2}, i.e., the upper bound of the first stopband, is given by the first root of (5b) and $f_s < f_{c2} < f_l$.

3) For $f_s > f_l$ (Fig. 3b), the second cutoff frequency f_{c2} is equal to f_l (first root of (5c)).

4) Fig. 3(a) and (b) shows that the stopband width increases with increasing impedance ratios ρ. In the particular case $\rho = 1$ $(r_s = r_l)$, explicit expressions for the cutoff

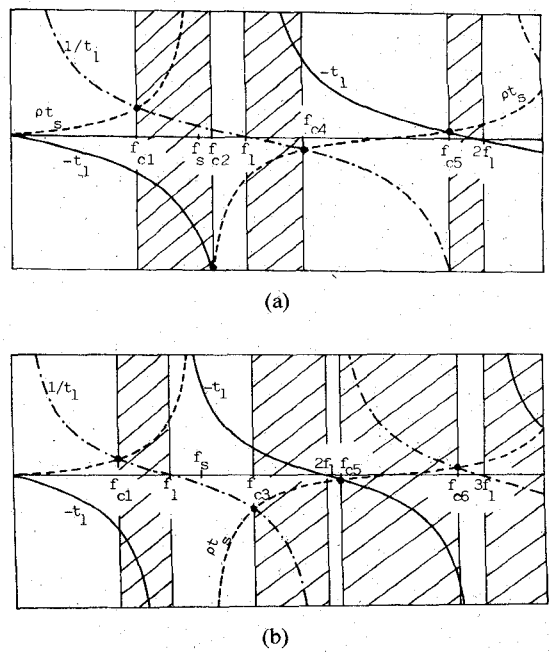

Fig. 3. Graphical solution for the cutoff frequencies for (a) $f_s < f_l$ and (b) $f_s > f_l$.

frequencies are obtainable from (5) as follows:

$$f_{c1} = f_s f_l/(f_s + f_l)$$
$$f_{c2} = \begin{cases} 2f_{c1}, & \text{for } f_s < f_l \\ f_l, & \text{for } f_s > f_l \end{cases}$$

The maximum percent stopband width $2(f_{c2} - f_{c1})/(f_{c2} + f_{c1})$ is, therefore, 67 percent and is obtained for $f_s < f_l$. It is interesting to note that this bandwidth is independent of f_s and f_l as long as $f_s < f_l$ and only for $\rho = 1$. Wider stopband widths can be obtained for higher ρ values. For $\rho < 1, f_{c2}$ is always less than $2f_{c1}$.

5) Some peculiarities occur in the commensurate case $f_s = f_l$. In the noncommensurate case, in fact, the image attenuation $\alpha = \mathrm{Re}(\gamma)$ has poles located at multiples of f_s: these poles correspond to the stub length being an odd multiple of a quarter of wavelength and, obviously, are located within the stopbands. For $f_s = f_l$, on the contrary, the image attenuation is always finite. Nevertheless, when the cell is terminated by resistances, transmission zeros occur at $f = mf_s$ $(m = 1,2,\ldots)$. This is due to the fact that the image impedance Z_{Is} has poles at these frequencies. Transmission zeros are obtained, in fact, either for $\alpha = \infty$ or for α finite and $Z_{Is} = \infty$. These two cases correspond, as can be easily demonstrated, to the interaction and modal transmission zeros, respectively, as discussed in [4].

It must furthermore be observed that for $f_s = f_l$, the cutoff frequencies are only those corresponding to the roots of (5a), which reduces to

$$\tan^2\left(\frac{\pi}{2}f/f_s\right) = 1/\rho.$$

The cutoff frequencies f_{c1} and f_{c2} are symmetrically located with respect to $f_l = f_s$. In particular, for $\rho = 1$, it results

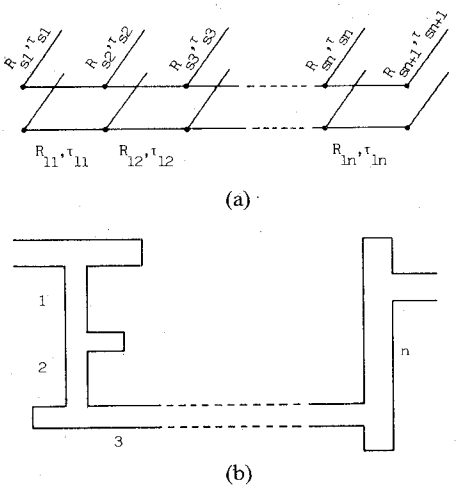

Fig. 1. (a) The distributed filter prototype and (b) the microstrip filter geometry.

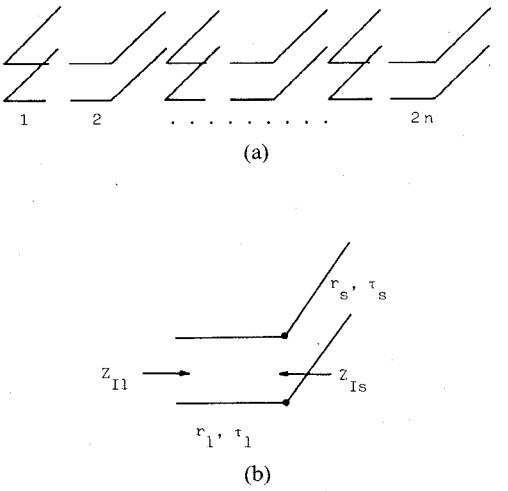

Fig. 2. (a) Reduction of Fig. 1(a) into the cascade of elementary cells. (b) The elementary cell.

In this paper, we show the application of the IPM to the design of a class of distributed low-pass filters. These filters were previously designed on a low-frequency approximation basis [2], [3], which did not allow control of the stopband behavior. The IPM, on the contrary, is shown to provide a control of both the passband and stopband behavior of the distributed prototype, leading to filters with improved overall characteristics, as also demonstrated by the experimental results.

II. The Filter Structure

In a previous work [2], it has been shown that low-pass filters with an elliptic-function response can be designed using the distributed prototype of Fig. 1(a). A low-frequency approximation was used to reduce the design procedure to the synthesis of an equivalent lumped prototype. In this manner, excellent passband behavior and high cutoff rates were obtained [3]; but, because of the approximation involved, no control of the stopband behavior was possible. The IPM can be used to overcome this limitation.

In the practical realization of Fig. 1(a) as a microstrip filter, it is convenient to reduce discontinuities at the connections between lines and stubs by imposing at each connection the equality of two of the three characteristic impedances. With reference to the notation of Fig. 1(a), one of the following conditions is imposed:

$$R_{l,i-1} = R_{s,i} \qquad \text{(L condition)} \qquad (1a)$$

or

$$R_{l,i-1} = R_{l,i} \qquad \text{(F condition)} \qquad (1b)$$

or

$$R_{s,i} = R_{l,i} \qquad \text{(R condition)} \qquad (1c)$$

$i = 1,2,\ldots, n+1$, where $R_{l0} = R_{l,m+4} = R_0$ are the characteristic impedances of the feeding lines.

Conditions (1a) or (1c) correspond to the stub having the same characteristic impedance as one of the adjacent lines and have been adopted in [2] and [3]. The consideration of (1b) generalizes the geometry of the microstrip filter as sketched in Fig. 1(b): its application, as will be shown later on, permits higher impedance ratios between lines and stubs to be obtained so as to increase the filter stopband. For the sake of clarity, in the sketch of Fig. 1(b), the three conditions (1) are imposed in the same order to the first three stubs.

Classical synthesis methods applied to the distributed prototype of Fig. 1(a) lead to commensurate structures. In such cases, the characteristic impedances are chosen as the free parameters of the synthesis. In the present case, however, the constraints (1) on the characteristic impedances render these methods inapplicable.

As is known, the IPM of filter design requires a number of elementary cells to be cascaded together in order to obtain the prescribed filter performance. By splitting each internal stub into the parallel of two stubs of the same length, and each line section into a series of two line sections with the same characteristic impedance, the scheme of Fig. 1(a) is converted into that of Fig. 2(a): this scheme consists of the cascade of $2n$ elementary cells of the type shown in Fig. 2(b). The IPM representation of the elementary cell is discussed in the next section, while the filter design procedure is presented in Section IV.

It is worth noting that a planar approach [4], [5] would be the most appropriate technique, particularly at high frequencies, to model the microstrip structure of Fig. 1(b). For the purposes of the present paper, however, a transmission-line model is adopted, as it is much simpler and, therefore, more suitable to demonstrate the effectiveness of the method. In any case, once the prototype of Fig. 1(a) has been designed, a planar approach has to be used to accurately transform Fig. 1(a) into Fig. 1(b)

III. Image Parameter Characterization of the Elementary Distributed Cell

The elementary cell of Fig. 2(b) is characterized in terms of four parameters, namely two characteristic impedances r_l and r_s and two delay times τ_l and τ_s. Its image imped-

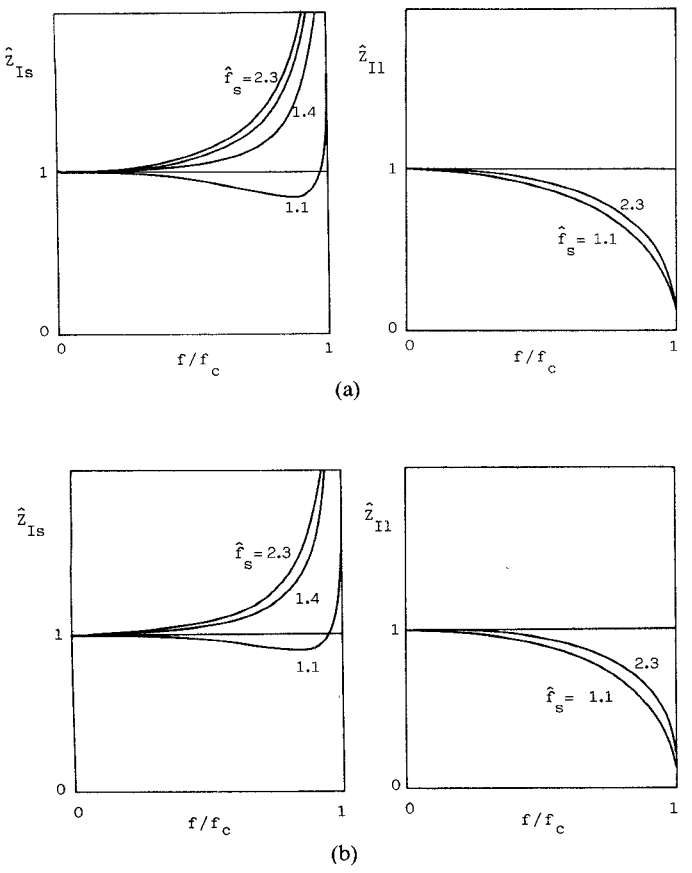

Fig. 4. Image impedances of the elementary cell versus the normalized frequency for (a) $\rho = 1$ and (b) $\rho = 0.5$.

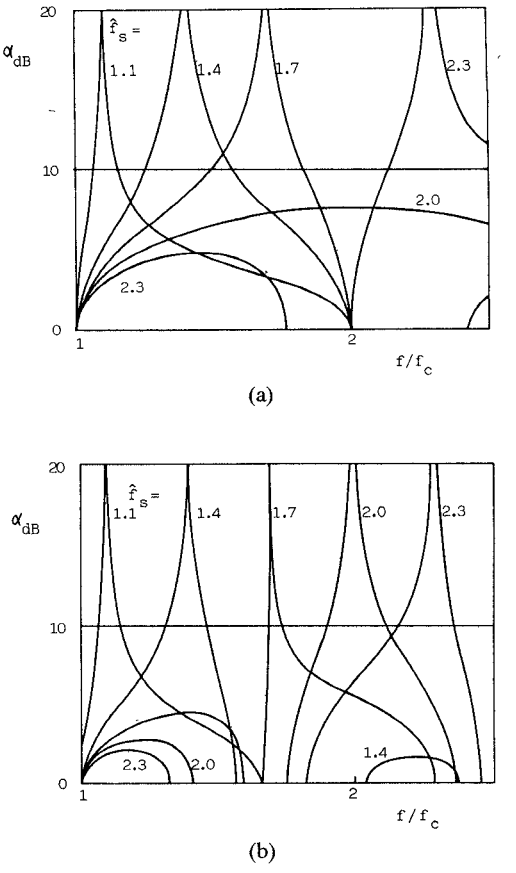

Fig. 5. Image attenuation of the elementary cell versus the normalized frequency (a) for $\rho = 1$ and (b) $\rho = 0.5$

$f_{c1} = f_s/2, f_{c2} = 3f_{c1}$. For a given ρ, the commensurate cell provides the maximum stopband width, but the image attenuation is limited; as f_s is made different from f_l, the stopband is split into two stopbands separated by a passband.

6) In the limit of zero frequency, the image impedances tend to the same value

$$K = \lim_{f \to 0} Z_{Il} = \lim_{f \to 0} Z_{Is} = r_l\left[1 + (r_l\tau_s)/(r_s\tau_l)\right]^{-1/2}. \quad (8)$$

To establish a design procedure for low-pass filters, it is convenient to characterize the elementary cell in terms of the first cutoff frequency f_{c1}, the impedance level K, the first transmission zero frequency f_s, and the impedance ratio ρ. In order to compare the image behavior of different cells, the same values of the cutoff frequency f_{c1} and impedance level K are assumed. In this mannner, the remaining two parameters f_s and ρ can be used to characterize the image properties of the cells.

From now on, we will consider the image impedances as normalized with respect to their zero frequency value K, and the frequencies with respect to the cutoff frequency f_c. A caret will be used to indicate normalized quantities. In order to simplify the notation, f_{c1} will be simply indicated as f_c.

The passband behavior of the normalized image impedances $\hat{Z}_{Is}$ and $\hat{Z}_{Il}$ and of the image attenuation $\alpha = \mathrm{Re}(\gamma)$ of the elementary cell are shown in Figs. 4 and 5 versus the normalized frequency $\hat{f}$ for different values of the transmission zero frequency $\hat{f}_s$ and the impedance ratio ρ.

It is noted that, as the cutoff frequency is approached, the image impedance at the line end Z_{Il} tends to zero, while the image impedance at the stub end Z_{Is} goes to infinity. Because of the different behaviors of Z_{Il} and Z_{Is} near f_c, contiguous elementary cells have to be cascaded as in Fig. 2(a), i.e., in reversed position, in order that the matching condition of the filter is guaranteed in the passband.

As the transmission zero frequency f_s, thus the stub length, is varied, only Z_{Is} is changed appreciably, while Z_{il} remains practically unchanged. It could be further shown that both Z_{Il} and Z_{Is} are slightly dependent on ρ. Because of these properties, the connection between different elementary cells gives rise to very small mismatchings, even if the image impedances are not exactly coincident.

Different behaviors of α are obtained depending on the values of ρ and $\hat{f}_s$. As previously noted, higher ρ values permit wider stopbands. Fig. 5 shows that, as long as $\hat{f}_s$ is less than a critical value, a pole of α is located in the first stopband. As stated in point 5) of the previous discussion, this critical value is nothing but $\hat{f}_l$. As $\hat{f}_s$ is raised above $\hat{f}_l$, the first stopband is reduced and the pole of α is located in

a second stopband. For f_s equal to f_l, no pole of α occurs.

It is now possible to put into evidence the main differences between the classical IPM application to lumped filters and the present one. In the classical IPM

1) each cell has a finite number of passbands and stopbands;
2) all the cells to be cascaded have the same cutoff frequency and the same location of passbands and stopbands;
3) the image impedances of adjacent cells are exactly coincident at all frequencies;
4) the filter behavior can be calculated in terms of image parameters both in the passband and in the stopband; in the case of low-pass filters, the latter extends up to infinity.

In the present application of the IPM

1) each cell has an infinite number of passbands and stopbands;
2) all the cells have the same fundamental cutoff frequency f_c, but the higher cutoff frequencies are generally different;
3) the image impedances of adjacent cells are not exactly coincident at all frequencies;
4) the filter behavior can be computed in terms of image parameters of the constituting cells only in the (first) passband and in the first part of the stopband; at higher frequencies, where some cells are in a passband and some others in a stopband, the filter must be characterized through the computation of the scattering parameter s_{21}.

IV. Design Procedure

The filter structure of Fig. 1(a) is built up by cascading a number of elementary cells individually image-matched in the passband. In doing this, three types of conditions must be imposed to the elementary cell parameters in order to satisfy the cascade constraints, the impedance constraints (1), and the matching of the cells:

A. Cascadability

In order that Fig. 2(a) could be reduced to Fig. 1(a), the equality must be imposed between the line characteristic impedances of two cells connected by the line ends and, similarly, between the stub delay times of two cells connected by the stub ends

$$r_{l,2i-1} = r_{l,2i}, \qquad i = 1,2,\ldots,n \tag{9a}$$

$$\tau_{s,2i} = \tau_{s,2i+1}, \qquad i = 1,2,\ldots,n-1. \tag{9b}$$

B. Impedance Constraints

The application of conditions (1) yields

$$r_{s1} = R_0 \quad \text{or} \quad r_{l1} = R_0 \quad r_{l1} = r_{s1} \tag{10a}$$

for the first stub

$$(r_{s,2i} // r_{s,2i+1}) = r_{l,2i} \quad \text{or} \quad r_{l,2i} = r_{l,2i+1}$$
$$\text{or} \quad (r_{s,2i} // r_{s,2i+1}) = r_{l,2i+1}, \qquad i = 1,2,\cdots,n-1 \tag{10b}$$

for the internal stubs, and

$$r_{s,2n} = r_{l,2n} \quad \text{or} \quad r_{l,2n} = R_0 \quad \text{or} \quad r_{s,2n} = R_0 \tag{10c}$$

for the last stub.

C. Image-Matching

Cells with equal (or as close as possible) image impedances must be cascaded together. This requires that all the cells have the same cutoff frequency f_c and the same K

$$f_{c,i} = f_{c,i+1}, \qquad i = 1,2,\cdots,2n-1 \tag{11a}$$

$$K_i = K_{i+1}, \qquad i = 1,2,\cdots,2n-1. \tag{11b}$$

We, therefore, have to impose $7n-2$ conditions on the $2n$ elementary cells. Since each cell is characterized by four parameters, the free parameters of the synthesis procedure are $8n-(7n-2) = n+2$. Among these are the filter cutoff frequency f_c and the impedance level K. When these quantities have been fixed for the entire filter structure, n free parameters are left to the design procedure, which is described thereafter.

As the passband behavior of the filter is automatically guaranteed by the IPM itself (apart from mismatchings at the band edges due to resistive terminations), the classical IP design procedure consists of cascading a number of cells to obtain the required stopband performance. This procedure is justified by virtue of the following properties.

1) The filter image attenuation α equals the sum of the individual image attenuations, which are generally known by tables or graphs.

2) For high attenuations, $|s_{21}|$ is well approximated by $-\alpha$ (using dB).

Also in the present case, the filter can be designed on the basis of the individual α's, plotted in Fig. 5. Since the filter possesses n degrees of freedom, n transmission zeros out of $n+1$ can be chosen to optimize the stopband behavior.

The design procedure can be carried out automatically on a computer and consists of the following steps.

1) Choose an initial set of n transmission zeros in the stopband.

2) Solve the system of equations (9)–(11) to determine the $(n+1)$th zero and the filter structure.

3) Analyze the filter to compute $|s_{21}|$.

4) Change the frequency location of the n transmission zeros according to some optimization strategy and go to step 2) until the stopband requirements are satisfied.

In the case of low-order filters ($n \leq 3$), the procedure can be implemented very easily on a desk-top computer and run in a few seconds. It is worth noting that, contrary to the classical application of the IPM, the approximation $|s_{21}| = -\alpha$ is not used, but $|s_{21}|$ is computed exactly from the filter parameters.

We conclude this section with some remarks about the choice of the value of the impedance level K. As could be easily seen, the zero frequency attenuation is always zero even if $K \neq R_0$. If $K = R_0$, a maximally flat response is obtained, but K values different from R_0 may also be chosen. This possibility is generally excluded for lumped filters, but, in the present case, it can be usefully adopted

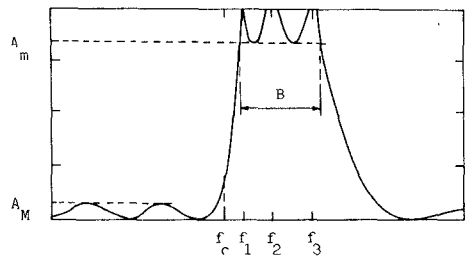

Fig. 6. Attenuation behavior of a fifth-order filter.

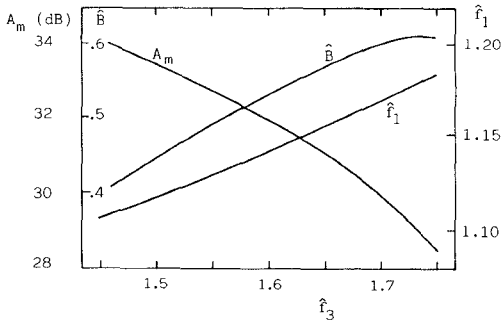

Fig. 7. Characteristics of optimized RLL filters versus the third transmission zero $\hat{f}_3$.

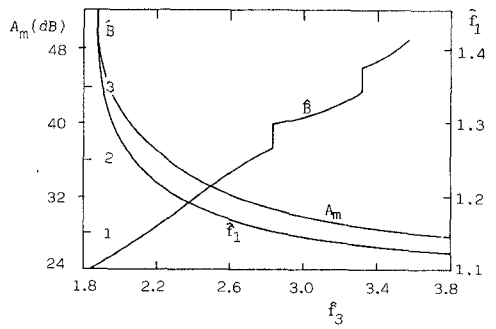

Fig. 8. Same as Fig. 7, but for RFR filters.

in order to improve the stopband behavior and/or render the component values more favorable for the practical construction of the filter. This is paid, of course, in terms of a higher passband attenuation. It is found that, for $K > 0.6\ R_0$, the passband attenuation is generally lower than 1.5 dB. The possibility of using K values different from R_0 depends on the characteristics of the distributed filters which seem to have intrinsically better performances than lumped-element filters.

For the sake of clarity, the next section illustrates in detail the features of the synthesis of some fifth-order filters. These filters correspond to the case of $n = 2$; thus, they are composed of four elementary cells and have three transmission zeros. Although the order of a distributed filter is somewhat arbitrary, we classified these filters by analogy with elliptic filters [2]; thus, the order M is given by $2n + 1$.

V. Fifth-Order Filters ($n = 2$)

The attenuation behavior of a fifth-order filter is schematically shown in Fig. 6. The filter possesses three transmission zeros $\hat{f}_1 \le \hat{f}_2 \le \hat{f}_3$ which determine the stopband characteristics in terms of the minimum attenuation A_m and the relative bandwidth $\hat{B} = B/f_c$. A_M is the maximum passband attenuation.

The filter is composed of $2n = 4$ elementary cells. Following the procedure outlined in the previous section, we choose $\hat{f}_1$ and $\hat{f}_3$ as the free parameters and apply (9)–(11) to determine $\hat{f}_2$ and the quantities R_{si}, τ_{si} $(i = 1,2,3)$, R_{li}, τ_{li} $(i = 1,2)$ defining the filter structure. An optimization procedure is then applied to obtain an equiripple stopband response. In practice, this procedure simply consists in determining, through (9)–(11), for each given $\hat{f}_3$, the value of $\hat{f}_1$ such that an equiripple response is obtained.

This procedure has been applied to two different classes of fifth-order filters, corresponding to two different choices in (1). The first class, which will be denoted as RLL, is obtained imposing conditions (1c), (1a), (1a) at the three connections between the four cells, while the second class, which will be denoted as RFR, results from the application of (1c), (1b), (1c). The corresponding microstrip geometries are shown in the insets of Figs. 9 and 10, respectively.

The results of the optimization procedure for the two classes are summarized in Figs. 7 and 8, respectively, where $\hat{f}_1$, $\hat{B}$, and A_m are plotted versus $\hat{f}_3$. It is seen that, as the third transmission zero $\hat{f}_3$ is increased, wider stopbands are obtained in both cases, at the price of lower stopband attenuations. The comparison between the two figures shows the substantially wider stopbands of the RFR filters. The component elementary cells of RLL filters, in fact, have ρ values typically less than unity. As a consequence, as discussed in Section III, the stopband cannot exceed unity. The use of condition (1b) in RFR filters, on the contrary, permits higher ρ values to be attained so that, as shown in Fig. 8, this limitation is removed. The peculiar discontinuous behavior of the bandwidth $\hat{B}$ of RFR filters is due to the occurrence of additional transmission zeros for specific values of $\hat{f}_3$. These higher order transmission zeros correspond to stubs being $3\lambda/4$ long, and are located at $3\hat{f}_1$, $3\hat{f}_2$.

Some low-pass filters designed according to this procedure have been fabricated in a microstrip configuration using an alumina substrate 0.635 mm thick and with dielectric permittivity $\epsilon_r = 10$.

The theoretical and experimental attenuation of an RLL filter is shown in Fig. 9 in the frequency range 2–14 GHz. Theoretical values have been computed through a planar analysis. The filter has been designed with a cutoff frequency $f_c = 6$ GHz, and with $K = 50\ \Omega$, corresponding to the feeding lines' impedance. It can be noted that the filter has a very high cutoff rate.

An example of a RFR filter is shown in Fig. 10. This filter has been designed with a cutoff frequency of 4 GHz and with an impedance level $K = 0.8R_0$ $(R_0 = 50\ \Omega)$. A very wide stopband, extending up to ~ 9.5 GHz, is observed. It is worth specifying that such wide stopbands in this type of filter are obtained by virtue of the high ρ values of the central cells of the prototypes, thus, of the

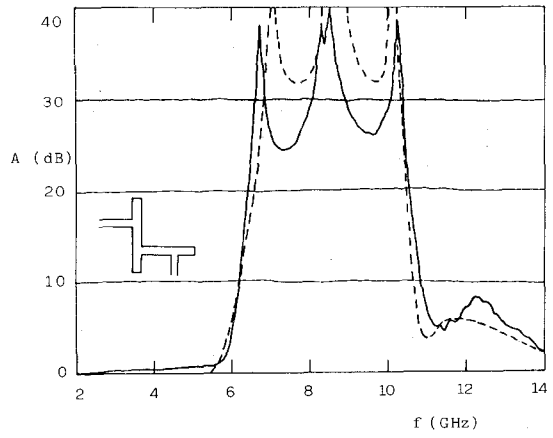

Fig. 9. Theoretical (planar analysis, dashed line) and measured (continuous line) attenuation of a microstrip RLL filter.

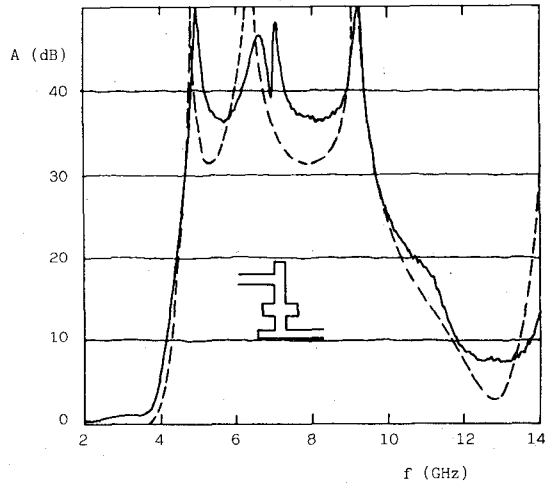

Fig. 10. Theoretical (planar analysis, dashed line) and measured (continuous line) attenuation of a microstrip RFR filter.

low impedances of the central stub. In a 50-Ω system, R_{s2} values are typically as low as 10–20 Ω. In the microstrip realization of these filters, it is, therefore, convenient to use parallel stubs, as shown in the inset of Fig. 10. In any case, as the widths of the stubs are generally not negligible, the dimensions are to be adjusted using a planar model analysis of the structure [5].

VI. Conclusions

The direct application of the IPM to distributed structures has been suggested in order to overcome some limitations of classical design methods for microwave filters. Several advantages can be obtained.

1) The IPM permits the design of noncommensurate distributed structures, while many classical methods lead to commensurate structures; thus, they do not utilize all their degrees of freedom.

2) The IPM can be applied directly to the microwave structure without any explicit or implicit use of lumped prototypes. This avoids errors or approximations in the transformation of the prototype into the microwave filter.

3) Since both characteristic impedances and delay times are used in the design, possible technological limitations, particularly on the characteristic impedances, can be incorporated in the design procedure.

4) Filters designed according to the IPM are internally matched in the passband; thus, they can be cascaded together in order to improve their characteristics.

To illustrate the features of the method and demonstrate its effectiveness, an application to the design of two classes of low-pass microstrip filters has been shown. Obviously, many other classes of filters can also be designed by simply removing or replacing some of the conditions used in the present application, namely, impedance constraints, cascade constraints, or the coincidence of the cutoff frequencies of the elementary cells. This would give additional degrees of freedom to the design.

It is finally worth observing that the application of the IPM is made very easy by modern computing facilities. In the examples presented, the design procedure has been implemented on a desk-top computer; the design of a fifth-order low-pass filter requires no more than a few seconds.

References

[1] G. L. Matthaei, L. Young, and E. M. T. Jones, *Microwave Filters Impedance-Matching Networks and Coupling Structures*. New York: McGraw-Hill, 1964.

[2] M. Salerno and R. Sorrentino, "Synthesis of low-pass elliptic filters for MIC as a class of non-commensurate distributed circuits," in *1982 IEEE MTT-S Int. Microwave Symp. Dig.* (Dallas, TX), June 1982, pp. 402–404.

[3] F. Giannini, M. Salerno, and R. Sorrentino, "Design of low-pass elliptic filters by means of cascaded microstrip rectangular elements," *IEEE Trans. Microwave Theory Tech.*, vol. MTT-30, pp. 1348–1353, Sept. 1982.

[4] G. D'Inzeo, F. Giannini, C. M. Sodi, and R. Sorrentino, "Method of analysis and filtering properties of microwave planar networks," *IEEE Trans. Microwave Theory Tech.*, vol. MTT-26 pp. 462–471, July 1978.

[5] R. Sorrentino, "Planar circuit, waveguide models, and segmentation method," *IEEE Trans. Microwave Theory Tech.*, vol. MTT-33, pp. 1057–1066, Oct. 1985.

Mario Salerno (M'84) was born in Rome, Italy, on March 30, 1944. He received a degree in electronic engineering from the University of Rome, Rome, Italy, in 1967.

Since 1970, he has been an Assistant Professor at the Institute of Electrical Communications of University of Rome. He was also an Associate Professor of Circuit Analysis at the University of Ancona, Ancona, Italy, from 1974 to 1976. He is presently an Associate Professor at the University of Rome. His research activities cover the field of general circuit theory and applications, filter design, digital signal processing, and microwave techniques.

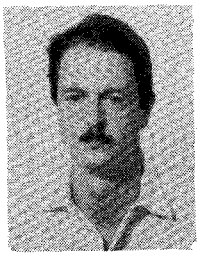

Roberto Sorrentino (M'77–SM'84) received the Laurea degree in electronic engineering from the University of Rome La Sapienza, Rome, Italy, in 1971.

He then joined the Institute of Electronics of the same university under a fellowship of the Italian Ministry of Education. Since 1974, he has been an Assistant Professor of Microwaves at Rome University La Sapienza. He was also professore incaricato of Microwaves at the University of Catania, Catania, Italy, from 1975 to 1976, and of the University of Ancona, Ancona, Italy, from 1976 to 1977. From 1977 to 1981, he was professore incaricato of Solid State Electronics at the University of Rome La Sapienza, where he is presently an Associate Professor of Microwave Measurements. From September to December 1983, he was appointed as a Research Fellow in the Electrical Engineering Department of the University of Texas at Austin, Austin, TX. His research activities have been concerned with electromagnetic wave propagation in anisotropic media, electromagnetic field interaction with biological tissues, and mainly with the analysis and design of microwave and millimeter-wave integrated circuits.

Since 1978, Dr. Sorrentino has been a member of the Executive Committee of the IEEE Middle and South Italy Section, and is the Chairman of the local MTT Chapter. He is also a member of the Italian Electrical Society (AEI).

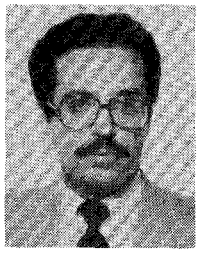

Franco Giannini (M'82–SM'84) was born in Galatina, Lecce, Italy, on November 9, 1944. He received the degree in electronic engineering from the University of Rome, Rome, Italy, in 1968.

In 1968, he joined the Institute of Electonics, University of Rome, where he had been an Assistant Professor until 1980. He was also an Associate Professor of Microwaves at the University of Ancona, Ancona, Italy, from 1973 to 1974, and of Solid-State Electronics at the University of Rome from 1974 to 1977. From 1977 to 1980, he had been an Associate Professor of Applied Electronics at the same university. In 1980, he became a Full Professor of Applied Electronics at the University of Rome, and since 1981 he has been with the Second University of Rome, Tor Vergata, where he is presently head of the Department of Electronic Engineering. He has been working on problems concerning theory and technology of active and passive microwave components, including GaAs monolithic circuits.

Dr. Giannini is a member of the Italian Electrical Society (AEI).